Modeling and Mechanism Analysis for New High-frequency Oscillation Phenomenon in MMC-HVDC Connected to AC Networks

Jieyi Xu, *Graduate Student Member*, *IEEE*, Hui Qin, Wenkai Dong, Juan Chen, and Xiaorong Xie, *Fellow*, *IEEE*

***Abstract*—High-frequency oscillations (HFOs) in modular multilevel converter based high-voltage direct current (MMC-HVDC) connected to AC networks have aroused concern in recent years. This paper reveals a new HFO phenomenon, where modular multilevel converter (MMC) exhibits impedance characteristics different from those in conventional HFO studies. To investigate this issue, a high-frequency dynamic model of MMC incorporating delay compensation is developed under different outer-loop control strategies. In addition, an AC line modeling method accounting for frequency-dependent parameters is proposed. Mechanism analysis demonstrates that the new HFO phenomenon arises from the adverse interaction between capacitive impedance of MMC and inductive impedance of AC network. Further, the causes of two types of capacitive regions in the high-frequency impedance of MMC are theoretically explained, which are linked to the relatively high proportional gains of current and power controls, as well as delay compensation. The effects of the frequency dependence of AC line parameters on HFO analysis are also demonstrated. Finally, the potential multiple HFOs and possible mitigation approaches are discussed for further study.**

***Index Terms*—Delay compensation, dynamic model, frequency-dependent parameter, impedance, high-frequency oscillation (HFO), AC network, modular multilevel converter based high-voltage direct current (MMC-HVDC).**

I. Introduction

MODULAR multilevel converter based high-voltage direct current (MMC-HVDC) technology has been developed rapidly due to its controllability, large-scale transmission capability, and high power quality [1], [2]. However, several high-frequency oscillation (HFO) events in MMC-HVDC connected to AC networks have occurred in worldwide projects such as the INFELFE project [3], Luxi back-to-back project [4], [5], and Yu'E back-to-back project [6]. These oscillations, with frequencies ranging from several hundred to several thousand hertz, pose challenges to system stability and reliability.

The HFO issues in MMC-HVDC are widely analyzed using impedance-based method. Existing literature points out that HFOs typically occur at frequencies where the modular multilevel converter (MMC) exhibits inductive impedance while the interconnected AC network exhibits capacitive impedance [5]-[10]. The influencing factors include time delay, controller parameters, and arm inductance of MMC, as well as AC line parameters. MMC control system typically experiences a long time delay, which is a critical factor inducing the negative damping of HFOs [8], [11]. It is also indicated that longer AC lines are more likely to expose MMC-HVDC to HFO risks, attributed to their capacitive behavior across multiple high-frequency regions [6], [8], [9]. Based on the above HFO mechanism, some targeted mitigation approaches have been proposed [9], [12], [13], mainly focusing on enhancing MMC damping in the capacitive regions of the interconnected AC networks, which are identified as risky regions of HFOs.

Existing studies generally recognize that the high-frequency impedance of MMC is predominantly inductive, primarily due to arm inductance [9]. However, the impact of control parameters on impedance characteristics remains relatively overlooked. Additionally, in some practical MMC-HVDC projects, delay compensation strategies are implemented in MMC control system to counteract the adverse effects of time delay on the fault ride-through capability of MMC [14], [15]. Nevertheless, existing literature of MMC modeling seldom incorporates such delay compensation. The influence of delay compensation on the high-frequency impedance of MMC remains unclear. Though [15] presented an MMC model with delay compensation, it neglected key elements such as voltage feedforward, thereby limiting the model generalizability. To date, the investigation of the high-frequency impedance of MMC is not comprehensive, which may hinder the accurate prediction of dynamic interactions in MMC-HVDC, potentially leading to unforeseen oscillation issues.

AC lines connected to MMC-HVDC also play a critical

Manuscript received: May 20, 2025; revised: August 14, 2025; accepted: September 15, 2025. Date of CrossCheck: September 15, 2025. Date of online publication: September 29, 2025.

This work was supported by the Science and Technology Project of Guangxi Power Grid Co., Ltd. (No. 046700KK52222037).

J. Xu, W. Dong, and X. Xie (corresponding author) are with the State Key Laboratory of Power System Operation and Control, Department of Electrical Engineering, Tsinghua University, Beijing 100084, China (e-mail: xujy22@mails.tsinghua.edu.cn; 596167281@qq.com; xiexr@tsinghua.edu.cn).

H. Qin and J. Chen are with Guangxi Power Grid Co., Ltd., Nanning 530023, China (e-mail: 517544316@qq.com; chen_j@gx.csg.cn).

DOI: 10.35833/MPCE.2025.000449

role in the occurrence of HFOs. In existing literature, high-frequency modeling of AC lines typically employs the Bergeron model [16] or multi-π-section model [6], [17], [18] to represent the distributed characteristics of line parameters. However, these models fail to account for the frequency dependence of AC line parameters caused by the skin effect, i. e., the per-unit-length resistance and inductance of overhead lines and cables vary with frequency [19] - [21]. This limitation can compromise the accuracy of HFO analysis. Analytical calculations for frequency-dependent line models require highly detailed structural and parametric data, making it very challenging for practical applications. To overcome this, [4] proposed a line model based on measured line parameters, which estimates parameters at specific high frequencies to reproduce HFO events, but it is not suitable for assessing system stability across a wide frequency range.

These gaps underscore the need for further research on high-frequency interactions between MMC-HVDC and AC network. The main contributions of this paper are as follows.

1) A high-frequency dynamic model of MMC incorporating delay compensation under different outer-loop control strategies is established. Additionally, a practical modeling method for AC lines that considers frequency-dependent parameters is proposed. They enable accurate characterization of the high-frequency dynamics of system components.

2) A new HFO phenomenon in MMC-HVDC connected to AC networks is revealed, with a mechanism different from previously studied HFOs. In high-frequency range, MMC can exhibit capacitive characteristics with negative resistance, and its interaction with AC network (behaving inductively) causes unstable HFOs. Both scenarios of MMC-HVDC connected to short and long AC lines are investigated.

3) Further investigation into impedance characteristics of MMC in high-frequency range is conducted. The root cause of two types of capacitive regions in high-frequency impedance of MMC is theoretically explained, and the key contributing factors are analyzed. Potential multiple HFOs and possible mitigation approaches are also discussed for further study.

The rest of the paper is organized as follows. Section II introduces the new HFO phenomenon in MMC-HVDC connected to AC networks. In Section III, the high-frequency dynamic models of MMC and AC network are developed. Section IV explains the mechanism of the new HFO phenomenon, analyzing the capacitive characteristics of MMC and the effects of frequency dependence of AC line parameters. Further, Section VII presents the potential multiple HFOs and discusses possible mitigation approaches. Conclusions are drawn in Section VII.

II. New HFO Phenomenon in MMC-HVDC Connected to AC Networks

A. System Description

In applications such as asynchronous AC grid interconnection and renewable energy transmission, MMC-HVDC is linked to AC grid via AC lines. Figure 1 presents a typical structure of such systems. The AC line length may be short or long, depending on the practical situations. Considering that the detailed modeling of the AC grid is not the focus of this study, for the purpose of analysis, it is modeled as a frequency-dependent impedance in series with a voltage source. Changes in the AC grid can be equivalently simulated by adjusting the series impedance. The main parameters of the test system are listed in Table I.

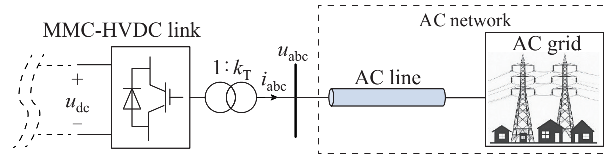

Fig. 1. MMC-HVDC connected to an AC network.

TABLE I
Main Parameters of Test System

Component	Parameter	Symbol	Value
MMC-HVDC	Voltage ratio of transformer	k_T	525 kV/375 kV
	Inductance of transformer	L_T	0.14 p.u.
	Proportional and integral parameters of power control	$k_{p,PQ}$, $k_{i,PQ}$	0.5, 16.7
	Proportional and integral parameters of DC voltage control	$k_{p,udc}$, $k_{i,udc}$	4, 100
	Proportional and integral parameters of current control	k_p, k_i	1, 33.3
	Inductance of arm	L_{arm}	0.040 H
	Time delay	T_d	300 μs
AC network	Line resistance at fundamental frequency of 50 Hz	R_1	0.017 Ω/km
	Line inductance at fundamental frequency of 50 Hz	L_1	0.866 mH/km
	Line capacitance	C_1	0.0134 μF/km
	Equivalent inductance of AC grid	L_g	0.0589 H

The control diagram of MMC is shown in Fig. 2, including outer-loop control, sequence separation, positive-sequence current control, negative-sequence current control, and time delay. Phase-locked loop (PLL) is not shown here due to space limitations. The outer-loop control includes power control and DC voltage control. The sequence separation adopts the delayed signal cancellation method [22], [23], with its transfer function expressed as $G_{pns}=(1+e^{-sT_{pn}})/2$, where T_{pn} is the time constant set as one-fourth of the fundamental frequency period. In Fig. 2, i_{dP}, i_{qP} and i_{dN}, i_{qN} are the positive- and negative-sequence dq components of AC-side current i_{abc} of MMC, respectively; u_{dP}, u_{qP} and u_{dN}, u_{qN} are the positive- and negative-sequence dq components of AC-side voltage u_{abc} of MMC, respectively; P and Q are the active power and reactive power, respectively; u_{dc} is the DC-side voltage of MMC; the superscript "ref" denotes the reference value; $G_{PQ}=k_{p,PQ}+k_{i,PQ}/s$, $G_{udc}=k_{p,udc}+k_{i,udc}/s$, and $G_i=k_p+k_i/s$ are the proportional-integral (PI) controller functions of power control, DC voltage control, and current control, respectively; $k_d=\omega_1 L$ is the decoupling coefficient in the current control, ω_1 is the fundamental angular frequency, and $L=L_T+L_{arm}/2$; and θ_{inv} is the phase angle for positive-sequence dq/abc transformation.

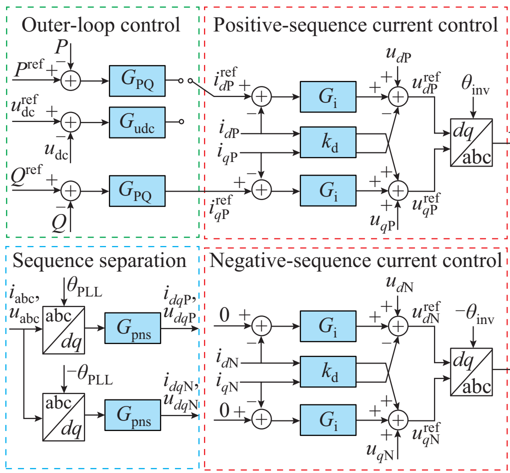

Fig. 2. Control diagram of MMC.

Practical MMC control system often suffers from long time delay, which stems from complex control strategies, extensive data communication between controllers, and switching delays of submodules. To reduce the adverse impact of time delay on the fault ride-through performance of the system, some practical MMC-HVDC projects have implemented delay compensation strategies. One implementation strategy is applying phase correction in the dq/abc transformation [14], [15]. Specifically, θ_{inv} is obtained by adjusting the output of PLL θ_{PLL}:

$$\theta_{inv}=\theta_{PLL}+\theta_0 \tag{1}$$

where $\theta_0=\omega_1 T_d$ is the compensation phase. The phase angle for the negative-sequence dq/abc transformation is $-\theta_{inv}$.

B. HFO Phenomenon

A detailed simulation model of the system shown in Fig. 1 is developed. The AC line is established using a typical frequency-dependent (phase) overhead line model in the simulation software. The DC side of MMC is connected to the opposite-side MMC-HVDC station via a DC line. Simulations of two typical scenarios are presented as follows. Note that the frequencies of HFOs discussed in this paper are above 500 Hz.

1) Scenario 1

This scenario investigates HFO when the MMC is connected to a relatively short AC line. The line length is set to be 3 km, and the MMC operates under power control with an active power output of 100 MW. The system is stable initially. At $t=1$ s, the proportional gain of current loop increases from 1 to 2.8, resulting in a gradually diverging oscillation. Figure 3 shows the AC-side current of MMC and its discrete fourier transform (DFT) analysis result. It is noted that the current contains an HFO component at 667 Hz.

2) Scenario 2

This scenario investigates HFO when the MMC is connected to a longer AC line. The line length is set to be 51 km, and the MMC is under power control with an active power output of 100 MW. Initially, the delay compensation in MMC is disabled, and the system is stable. However, an unstable HFO occurs at $t=1$ s after adding the delay compensation. The AC-side current of MMC and its DFT analysis result are shown in Fig. 4, indicating that the HFO frequency is around 3109 Hz.

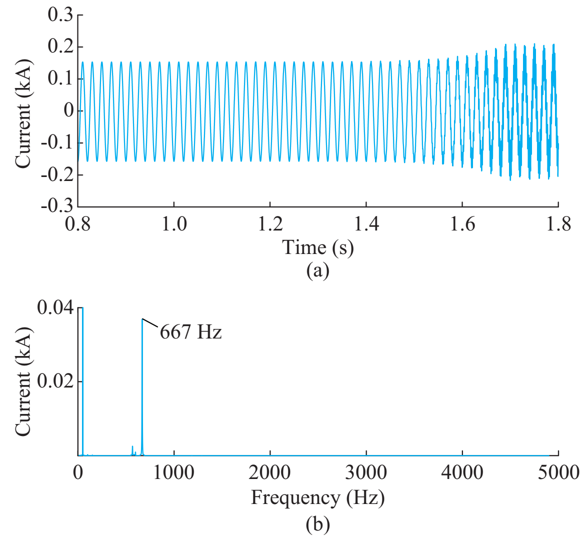

Fig. 3. AC-side current of MMC and its DFT analysis result in Scenario 1. (a) AC-side current waveform of MMC. (b) DFT analysis result.

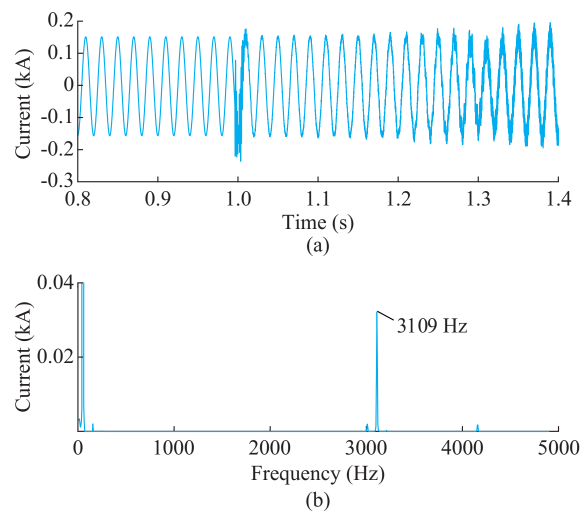

Fig. 4. AC-side current of MMC and its DFT analysis result in Scenario 2. (a) AC-side current waveform of MMC. (b) DFT analysis result.

C. Capacitive Characteristics of MMC

The equivalent impedance of MMC at the oscillation frequency can be identified using the simulation data [24], [25]. By performing DFT analysis on the voltage and current at the AC side of MMC, and extracting the phasors $\dot{V}_s$ and $\dot{I}_s$ at the oscillation frequency, the equivalent impedance of MMC is calculated as:

$$Z_s=\dot{V}_s/\dot{I}_s=R_s+jX_s \tag{2}$$

where R_s and X_s are the equivalent resistance and reactance at the oscillation frequency, respectively.

Table II displays the equivalent impedances of MMC at the oscillation frequency in Scenarios 1 and 2. Notably, MMC behaves as negative resistance ($R_s<0$) and capacitance ($X_s<0$) at the HFO frequencies. This contrasts with the typically inductive characteristics of MMC in existing studies on HFOs [5]-[10]. It reveals a new HFO phenomenon, indicating that MMC can also exhibit capacitive characteristics in high-frequency range and cause unstable HFOs. The discovery underscores the complexity of HFO dynamics in MMC-HVDC and necessitates further investigation.

TABLE II
EQUIVALENT IMPEDANCES OF MMC AT OSCILLATION FREQUENCY IN SCENARIOS 1 AND 2

Scenario	HFO frequency (Hz)	R_s (Ω)	X_s (Ω)
Scenario 1	667	−13.2	−254.9
Scenario 2	3109	−17612.2	−3736.4

III. HIGH-FREQUENCY DYNAMIC MODELS OF MMC AND AC LINE

A. Model of MMC

The harmonic linearization method is used to derive the AC-side high-frequency impedance of MMC. In high-frequency range, the dynamics of PLL and circulating current control are ignorable [5]. Due to the attenuation effects of the capacitors and inductors, the DC side of MMC is nearly immune to high-frequency disturbances from the AC side, so DC-side dynamics can be reasonably neglected when studying the AC-side high-frequency impedance [9]. Assuming a positive-sequence voltage disturbance V_p of frequency f_p is injected into the AC side of MMC, the phase-a voltage and current of MMC at the frequency f can be represented as:

$$\Delta u_a(f)=\begin{cases}\dot{V}_1 & f=f_1\\ \dot{V}_p & f=f_p\end{cases} \tag{3}$$

$$\Delta i_a(f)=\begin{cases}\dot{I}_1 & f=f_1\\ \dot{I}_p & f=f_p\end{cases} \tag{4}$$

where $\dot{V}_1$ is the voltage component at the fundamental frequency f_1; and $\dot{I}_1$ and $\dot{I}_p$ are the current components at f_1 and f_p, respectively.

According to the outer-loop control and current control structures depicted in Fig. 2, the expressions of the positive-sequence dq-frame voltage references can be obtained as:

$$\begin{cases}\Delta u_{dP}^{ref}(f)=M_{id}\dot{I}_p+M_{vd}\dot{V}_p & f=f_p-f_1\\ \Delta u_{qP}^{ref}(f)=M_{iq}\dot{I}_p+M_{vq}\dot{V}_p & f=f_p-f_1\end{cases} \tag{5}$$

where M_{id}, M_{iq}, M_{vd}, and M_{vq} are related to the outer-loop control strategy. For instance, their expressions under power control are given by:

$$\begin{cases}M_{id}=-1.5\dot{V}_1G_i^+G_{PQ}^+-(G_i^+-jk_d)G_{pns}^+\\ M_{iq}=j1.5\dot{V}_1G_i^+G_{PQ}^++(jG_i^++k_d)G_{pns}^+\\ M_{vd}=-1.5\dot{I}_1e^{-j\varphi_i}G_i^+G_{PQ}^++G_{pns}^+\\ M_{vq}=-j1.5\dot{I}_1e^{-j\varphi_i}G_i^+G_{PQ}^+-jG_{pns}^+\end{cases} \tag{6}$$

where φ_i is the phase difference between $\dot{V}_1$ and $\dot{I}_1$; the superscripts "+" and "−" of transfer functions denote the frequency shifts, such as $G^+=G(s-j\omega_1)$ and $G^-=G(s+j\omega_1)$.

Then, considering delay compensation, the phase angle for the positive-sequence dq/abc transformation is given by (1). Performing dq/abc transformation on (5), the expression of positive-sequence phase-a voltage is derived as:

$$\Delta u_{aP}^{ref}=0.5e^{j\theta_0}[(M_{id}+jM_{iq})\dot{I}_p+(M_{vd}+jM_{vq})\dot{V}_p+\Delta\theta(ju_{d0}-u_{q0})]\quad f=f_p \tag{7}$$

where u_{d0} and u_{q0} are the d- and q-axis voltage outputs of the current loop in steady state, respectively; and $\Delta\theta$ is the deviation angle of PLL output. Similarly, the negative-sequence phase-a voltage Δu_{aN}^{ref} can be derived.

Nearest level modulation (NLM) strategy is employed for the modulation process. In practical MMC-HVDC projects, the equivalent switching frequency is very high, and the harmonics in modulation process can be considered negligible [11]. Thus, the phase-a voltage output of MMC is expressed as:

$$\Delta u_a^{out}=G_d(\Delta u_{aP}^{ref}+\Delta u_{aN}^{ref}) \tag{8}$$

where $G_d=e^{-sT_d}$ represents the influence of time delay.

The circuit equation of AC side of MMC is:

$$\Delta u_a^{out}-\Delta u_a=sL\Delta i_a \tag{9}$$

By substituting (7) and (8) into (9), the AC-side high-frequency impedance model of MMC can be obtained as:

$$Z_{MMC}=\frac{\dot{V}_p}{\dot{I}_p}=\frac{sL+H_iG_d}{1-H_uG_d} \tag{10}$$

where H_i and H_u are the transfer functions that depend on the outer-loop control strategy. Under power control and DC voltage control, H_i and H_u are expressed as (11) and (12), respectively.

$$\begin{cases}H_i=(G_i^+G_{pns}^+-jk_dG_{pns}^+)e^{j\theta_0}+(G_i^-G_{pns}^-+jk_dG_{pns}^-)e^{-j\theta_0}+\\ \qquad 1.5\dot{V}_1G_i^+G_{PQ}^+e^{j\theta_0}\\ H_u=G_{pns}^+e^{j\theta_0}+G_{pns}^-e^{-j\theta_0}\end{cases} \tag{11}$$

$$\begin{cases}H_i=(G_i^+G_{pns}^+-jk_dG_{pns}^+)e^{j\theta_0}+(G_i^-G_{pns}^-+jk_dG_{pns}^-)e^{-j\theta_0}+\\ \qquad 0.75\dot{V}_1G_i^+G_{PQ}^+e^{j\theta_0}\\ H_u=G_{pns}^+e^{j\theta_0}+G_{pns}^-e^{-j\theta_0}-0.75G_i^+G_{PQ}^+(i_{d0}-ji_{q0})e^{j\theta_0}\end{cases} \tag{12}$$

where i_{d0} and i_{q0} are the d- and q-axis currents of MMC in steady state, respectively.

To verify the accuracy of MMC impedance model, frequency scanning is performed. Figure 5 presents the comparison of scanned and analytical impedances of MMC under different control strategies. Notably, the scanned and analytical results closely match in the high-frequency range of 500 Hz to 5000 Hz.

B. Model of AC Line Considering Frequency-dependent Parameters

In high-frequency range, the distributed model of AC line shown in Fig. 6 is adopted, where the line is composed of numerous infinitesimal elements dx. Given the typical insulation of lines, the line conductance is usually neglected. With an impedance Z_g at the receiving end of the line, the input impedance observed from the sending end of the line [4] is derived as:

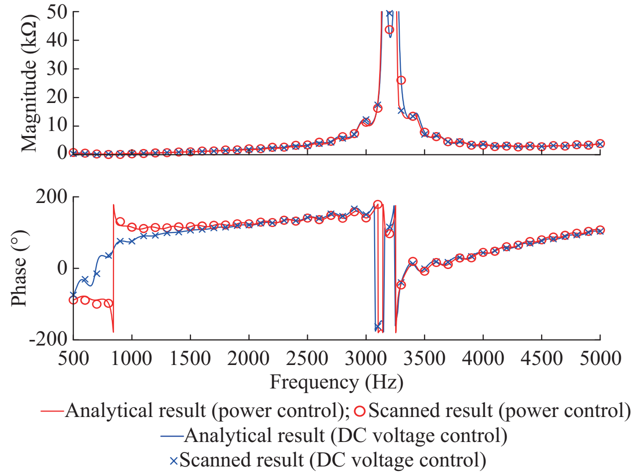

Fig. 5. Comparison of scanned and analytical impedances of MMC under different control strategies.

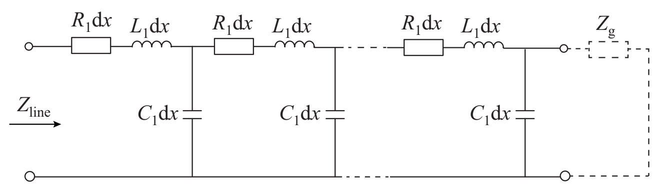

Fig. 6. Distributed model of AC line.

$$Z_{line}=\frac{Z_g+\sqrt{Z/Y}\tanh(\sqrt{ZY}\,l)}{1+Z_g/\sqrt{Z/Y}\tanh(\sqrt{ZY}\,l)} \tag{13}$$

where l is the length of the AC line; and $Z=R_1+j\omega L_1$ and $Y=j\omega C_1$ are the per-unit-length impedance and admittance of the AC line, respectively.

To accurately represent the high-frequency dynamics of AC lines, the frequency dependence of AC line parameters should be considered [4], [19], [20]. However, the analytical calculation of these frequency-dependent parameters is complex. For a balance between modeling accuracy and complexity, this paper utilizes a numerical approximation technique to represent the frequency response of line resistance and inductance. The procedure of the modeling method is given below.

Step 1: according to [26] and [27], the line resistance and inductance can be expressed as complex functions related to the square root of frequency. Here, polynomial functions are used to approximate these frequency responses:

$$\begin{cases} R_1(f)=a_n(\sqrt{f})^n+\dots+a_1\sqrt{f}+a_0 \\ L_1(f)=b_m(\sqrt{f})^m+\dots+b_1\sqrt{f}+b_0 \end{cases} \tag{14}$$

where n and m are the polynomial orders; and a_i ($i=0,1,\dots,n$) and b_j ($j=0,1,\dots,m$) are the coefficients of polynomial functions. The polynomial orders can be increased appropriately according to the required fitting accuracy.

Step 2: substitute the approximated frequency responses of resistance and inductance into (13), and the impedance model of the AC line that considers frequency-dependent parameters can be derived.

IV. Mechanism of New HFO Phenomenon

This section assesses system stability and explains the mechanism of the new HFO phenomenon. Further, a simplified impedance model of MMC is introduced to mathematically analyze its capacitive characteristics. The effects of frequency dependence of AC line parameters on HFO analysis are also examined.

A. Mechanism Explanation

Using the proposed modeling method, Fig. 7(a) presents the analytical impedances of MMC and AC network for Scenario 1.

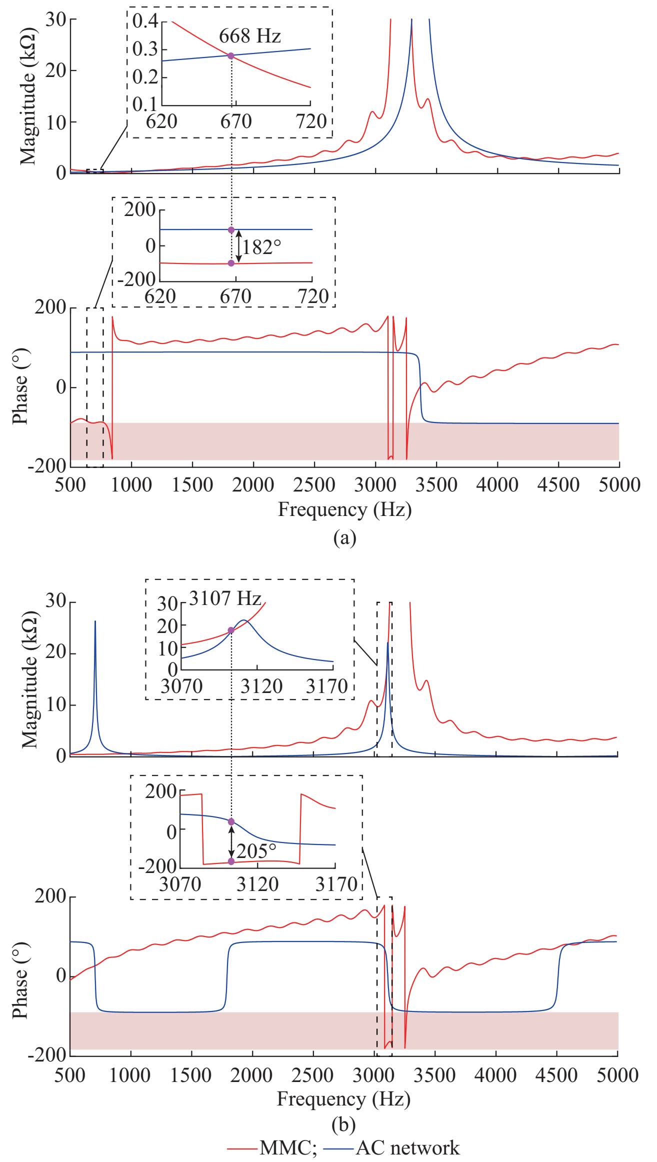

Fig. 7. Analytical impedances of MMC and AC network for Scenarios 1 and 2. (a) Scenario 1. (b) Scenario 2.

The red shaded area indicates that the impedance phase is between −180° and −90°, corresponding to capacitive and negative resistance characteristics. There is a magnitude intersection at 668 Hz. At this frequency, the phase of MMC impedance is −93°, suggesting characteristics of capacitance and negative resistance, and the phase of AC network impedance is about 89°. The phase difference between the two impedances exceeds 180° at 668 Hz, indicating a negatively damped HFO mode in the system, which agrees with the simulation results in Section II-B.

Figure 7(b) displays the analytical impedances of MMC and AC network for Scenario 2. A magnitude intersection is noted at 3107 Hz, where the phase of MMC impedance is –168° and the phase of AC network impedance is 37°, leading to a phase difference of 205°. Consequently, the system is unstable with the HFO frequency near 3107 Hz. This theoretical analysis is consistent with the simulation results in Section II-B.

Based on the above analysis, the mechanism of the new HFO phenomenon can be systematically explained as follows. At some high frequencies, MMC presents capacitive and negative-resistance characteristics while AC network impedance presents inductive characteristics, differing from those characteristics in existing HFO research. The interaction between MMC and AC network leads to the formation of an equivalent RLC resonance within the entire system, corresponding to an HFO mode. If the negative resistance of MMC is large enough to make the total system resistance negative, the HFO mode is unstable.

The occurrence conditions of the new HFO phenomenon deserve attention. Existing studies mainly focus on conventional HFO risks of MMC-HVDC with long AC lines, due to the capacitive behavior of lines at high frequencies. However, the newly identified HFO phenomenon can pose significant risks regardless of whether MMC-HVDC is connected to short or long AC lines. In scenarios with short AC lines, the first resonance peak of AC network impedance may be as high as several kilohertz. Below the first resonance peak, the AC network remains inductive across a wide frequency range and can form an HFO mode with the capacitive MMC impedance. In scenarios with long AC lines, AC network impedance may also exhibit multiple inductive regions above several hundred hertz. Thus, MMC could also face HFO risks within these inductive regions of AC network.

B. Analysis of Capacitive Characteristics of MMC

Previous analyses show that MMC impedances may exhibit two types of capacitive regions at frequencies above 500 Hz: the first appears in the frequency range of 500 Hz to 1000 Hz; while the second appears in the frequency range of several kilohertz, particularly near the frequency of impedance magnitude peaks. However, the origins of these risky regions remain unclear. To address this, it is necessary to further investigate Z_{MMC} depicted in (10).

For simplification, the effects of PLL can be ignored at frequencies above 500 Hz. The integral terms of current and power controllers are also neglected. Given that $G_\mathrm{i}^+ \approx G_\mathrm{i}^- \approx k_\mathrm{p}$ in high-frequency range, the term $(G_\mathrm{i}^+ G_\mathrm{pns}^+ - \mathrm{j}k_\mathrm{d} G_\mathrm{pns}^+)\mathrm{e}^{\mathrm{j}\theta_0} + (G_\mathrm{i}^- G_\mathrm{pns}^- + \mathrm{j}k_\mathrm{d} G_\mathrm{pns}^-)\mathrm{e}^{-\mathrm{j}\theta_0}$ in the numerator of Z_{MMC} can be simplified as:

$$\begin{aligned}
&(G_\mathrm{i}^+ G_\mathrm{pns}^+ - \mathrm{j}k_\mathrm{d} G_\mathrm{pns}^+)\mathrm{e}^{\mathrm{j}\theta_0} + (G_\mathrm{i}^- G_\mathrm{pns}^- + \mathrm{j}k_\mathrm{d} G_\mathrm{pns}^-)\mathrm{e}^{-\mathrm{j}\theta_0} \approx \\
&\quad k_\mathrm{p}(G_\mathrm{pns}^+ \mathrm{e}^{\mathrm{j}\theta_0} + G_\mathrm{pns}^- \mathrm{e}^{-\mathrm{j}\theta_0}) - \mathrm{j}k_\mathrm{d}(G_\mathrm{pns}^+ \mathrm{e}^{\mathrm{j}\theta_0} - G_\mathrm{pns}^- \mathrm{e}^{-\mathrm{j}\theta_0}) = \\
&\quad 0.5k_\mathrm{p}[\mathrm{e}^{\mathrm{j}\theta_0} + \mathrm{e}^{-\mathrm{j}\theta_0} + (\mathrm{e}^{\mathrm{j}(\omega_1 T_\mathrm{pn} + \theta_0)} + \mathrm{e}^{-\mathrm{j}(\omega_1 T_\mathrm{pn} + \theta_0)})\mathrm{e}^{-sT_\mathrm{pn}}] - \\
&\quad \mathrm{j}0.5k_\mathrm{d}[\mathrm{e}^{\mathrm{j}\theta_0} - \mathrm{e}^{-\mathrm{j}\varphi_0} + (\mathrm{e}^{\mathrm{j}(\omega_1 T_\mathrm{pn} + \theta_0)} - \mathrm{e}^{-\mathrm{j}(\omega_1 T_\mathrm{pn} + \theta_0)})\mathrm{e}^{-sT_\mathrm{pn}}] = \\
&\quad k_\mathrm{p}\cos(\theta_0) + k_\mathrm{d}\sin(\theta_0) + (-k_\mathrm{p}\sin(\theta_0) + k_\mathrm{d}\cos(\theta_0))\mathrm{e}^{-sT_\mathrm{pn}}
\end{aligned} \tag{15}$$

Similarly, the term $G_\mathrm{pns}^+ \mathrm{e}^{\mathrm{j}\theta_0} - \mathrm{j}G_\mathrm{pns}^+ \mathrm{e}^{\mathrm{j}\theta_0}$ in the denominator of Z_{MMC} can be simplified to $\cos(\theta_0) + \sin(\theta_0)\mathrm{e}^{-sT_\mathrm{pn}}$.

Then, by substituting $s = \mathrm{j}\omega$ into (10)-(12), Z_{MMC} can be reduced to:

$$Z_\mathrm{M} = \frac{A\cos(\omega T_\mathrm{d}) - B\sin(\omega T_\mathrm{d}) + \mathrm{j}(\omega L - A\sin(\omega T_\mathrm{d}) - B\cos(\omega T_\mathrm{d}))}{1 - C\cos(\omega T_\mathrm{d}) + D\sin(\omega T_\mathrm{d}) + \mathrm{j}(C\sin(\omega T_\mathrm{d}) + D\cos(\omega T_\mathrm{d}))} \tag{16}$$

where A, B, C, and D are the parameters that can be expressed as (17) under power control strategy or (18) under DC voltage control strategy.

$$\begin{cases}
A = k_\mathrm{p}\cos(\theta_0) + k_\mathrm{d}\sin(\theta_0) + \\
\quad (-k_\mathrm{p}\sin(\theta_0) + k_\mathrm{d}\cos(\theta_0))\cos(\omega T_\mathrm{pn}) + 1.5\dot{V}_1 k_\mathrm{p} k_\mathrm{p,PQ} \\
B = (-k_\mathrm{p}\sin(\theta_0) + k_\mathrm{d}\cos(\theta_0))\sin(\omega T_\mathrm{pn}) \\
C = \cos(\theta_0) + \sin(\theta_0)\cos(\omega T_\mathrm{pn}) \\
D = \sin(\theta_0)\sin(\omega T_\mathrm{pn})
\end{cases} \tag{17}$$

$$\begin{cases}
A = k_\mathrm{p}\cos(\theta_0) + k_\mathrm{d}\sin(\theta_0) + \\
\quad (-k_\mathrm{p}\sin(\theta_0) + k_\mathrm{d}\cos(\theta_0))\cos(\omega T_\mathrm{pn}) + 0.75\dot{V}_1 k_\mathrm{p} k_\mathrm{p,PQ}\cos(\theta_0) \\
B = (-k_\mathrm{p}\sin(\theta_0) + k_\mathrm{d}\cos(\theta_0))\sin(\omega T_\mathrm{pn}) - 0.75\dot{V}_1 k_\mathrm{p} k_\mathrm{p,PQ}\sin(\theta_0) \\
C = \cos(\theta_0) + \sin(\theta_0)\cos(\omega T_\mathrm{pn}) + \\
\quad 0.75 k_\mathrm{p} k_\mathrm{p,PQ}(i_{d0}\cos(\theta_0) + i_{q0}\sin(\theta_0)) \\
D = \sin(\theta_0)\sin(\omega T_\mathrm{pn}) - 0.75 k_\mathrm{p} k_\mathrm{p,PQ}(i_{d0}\sin(\theta_0) - i_{q0}\cos(\theta_0))
\end{cases} \tag{18}$$

The imaginary part of (16) corresponds to the equivalent impedance of MMC, which is expressed as:

$$\mathrm{Im}(Z_\mathrm{M}) = \frac{E_1 + E_2}{F} \tag{19}$$

$$\begin{cases}
E_1 = \omega L(1 - C\cos(\omega T_\mathrm{d}) + D\sin(\omega T_\mathrm{d})) \\
E_2 = -A\sin(\omega T_\mathrm{d}) - B\cos(\omega T_\mathrm{d}) + (BC - AD) \\
F = (1 - C\cos(\omega T_\mathrm{d}) + D\sin(\omega T_\mathrm{d}))^2 + \\
\quad (C\sin(\omega T_\mathrm{d}) + D\cos(\omega T_\mathrm{d}))^2
\end{cases} \tag{20}$$

Given that the compensation phase θ_0 is small, $\sin(\theta_0)$ is significantly smaller than $\cos(\theta_0)$, which implies that $C > 0$. E_1 can also be expressed as:

$$E_1 = \omega L(1 - \sqrt{C^2 + D^2}\cos(\omega T_\mathrm{d} + \beta)) \tag{21}$$

where $\beta = \arctan(D/C)$, which is a small angle because D is much less than C.

Notably, whether MMC presents capacitive or inductive characteristics is determined by the sign of $E_1 + E_2$. The magnitude of E_1 increases significantly with frequency (due to the term ωL) and is independent of the control parameters k_p and $k_\mathrm{p,PQ}$. In contrast, the magnitude of E_2 is prominently influenced by the control parameters k_p and $k_{p,PQ}$. The following analysis will explore the reasons for capacitive characteristics of MMC in two types of capacitive regions.

1) The First Type of Capacitive Region

The first type of capacitive region of MMC is located between 500 Hz and 1000 Hz. In this frequency range, the magnitude of E_1 is relatively small, and the effects of E_2 on MMC reactance cannot be ignored.

Equation (17) indicates that E_2 would be affected by k_p and $k_{p,PQ}$. The impact of k_p is analyzed as an example. According to (17), as k_p increases, A will increase mainly due to the terms $k_p\cos(\theta_0)$ and $s_c\dot{V}_1 k_p k_{p,PQ}$ ($s_c=1.5$ for power control and $s_c=0.75$ for DC voltage control), given that $\sin(\theta_0)$ is much smaller than $\cos(\theta_0)$. Thus, the term $-A\sin(\omega T_d)$ in E_2 becomes more negative, since $\sin(\omega T_d)>0$ in the frequency range of 500 Hz to 1000 Hz. Other terms in E_2 change relatively little compared with $-A\sin(\omega T_d)$. As a result, an increase in k_p leads to a decrease in E_2, potentially making E_1+E_2 below zero, which indicates capacitive characteristics of MMC. It is noteworthy that the s_c value depends on the outloop control strategy, with a larger s_c under power control. Consequently, the effects of k_p on the capacitive characteristics of MMC are more pronounced under power control. Similar analyses apply to the impact of $k_{p,PQ}$.

For instance, Fig. 8 illustrates the impedance-frequency curves of MMC with different values of k_p under different control strategies. The red shaded area indicates that the impedance phase is between $-180°$ and $-90°$, corresponding to capacitive and negative resistance characteristics. As k_p increases, the frequency at which MMC impedance transitions from capacitive to inductive becomes higher. In other words, the capacitive region of MMC expands. Additionally, higher k_p decreases MMC resistance in this frequency range, potentially causing a negative resistance region. Notably, the effects of k_p on the MMC impedance characteristics are more significant under power control than DC voltage control.

The above analysis indicates that, as k_p or $k_{p,PQ}$ increases, MMC is more likely to exhibit capacitive characteristics with negative resistance in the frequency range of 500 Hz to 1000 Hz, especially under power control. This will induce HFO risks when MMC is connected to an external inductive impedance.

2) The Second Type of Capacitive Region

The second type of capacitive region of MMC is situated at a higher frequency range of several kilohertz. In this frequency range, due to the large value of ωL, E_1 is significantly larger than E_2. Thus, capacitive characteristics of MMC are dominated by E_1, and the influence of E_2 becomes negligible. According to (16), the sign of E_1 is determined by the term $1-\sqrt{C^2+D^2}\cos(\omega T_d+\beta)$, which will be examined under different control strategies.

1) Under power control

It can be derived from (17) that $\sqrt{C^2+D^2}=\sqrt{1+\sin(2\theta_0)\cos(\omega T_{pn})}$. If the delay compensation is disabled (i.e., $\theta_0=0$), then $\sqrt{C^2+D^2}=1$ and $E_1=\omega L(1-\cos(\omega T_d))>0$. It indicates that MMC exhibits inductive characteristics across the frequency range of several kilohertz.

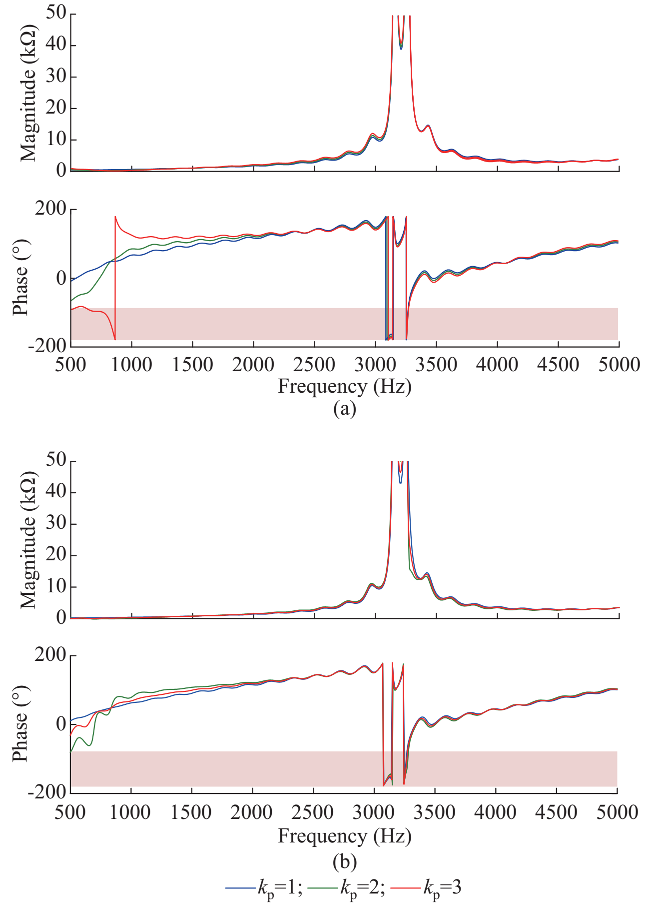

Fig. 8. Impedance-frequency curves of MMC with different values of k_p under different control strategies. (a) Under power control. (b) Under DC voltage control.

However, when delay compensation is applied (i. e., $\theta_0>0$), $\sqrt{C^2+D^2}$ may exceed 1 at frequencies where $\cos(\omega T_{pn})>0$. Meanwhile, since β is small, $\cos(\omega T_d+\beta)\approx 1$ is satisfied at frequencies near n/T_d (where n is a positive integer). Consequently, $1-\sqrt{C^2+D^2}\cos(\omega T_d+\beta)$, and thus E_1, may become negative at frequencies near n/T_d, indicating capacitive characteristics of MMC. Furthermore, at frequencies near n/T_d, it can be deduced that the denominator of Z_M in (16) approaches zero, leading to a significantly large magnitude of MMC impedance.

2) Under DC voltage control

Similarly, when $1-\sqrt{C^2+D^2}\cos(\omega T_d+\beta)$ becomes negative, it indicates capacitive characteristics of MMC. It is worth noting that under the DC voltage control, (18) shows that the values of C and D are related to the steady-state currents of MMC i_{d0} and i_{q0}. Given that $\cos(\theta_0)\gg\sin(\theta_0)$ and $|i_{d0}|\gg|i_{q0}|$, when MMC injects active power into the AC network ($i_{d0}>0$), the value of $\sqrt{C^2+D^2}$ is larger than that when $i_{d0}<0$. Therefore, at frequencies near n/T_d, where $\cos(\omega T_d+\beta)\approx 1$, the term $1-\sqrt{C^2+D^2}\cos(\omega T_d+\beta)$ is more likely to be negative when $i_{d0}>0$, indicating a higher propensity for capacitive regions of MMC in inverter mode. Furthermore, an increase in i_{d0} amplifies the value of $\sqrt{C^2+D^2}$, thereby expanding capacitive regions of MMC.

For an intuitive illustration, Fig. 9 compares MMC impedances with and without delay compensation for varying i_{d0} values under different control strategies. The red shaded area indicates that the impedance phase is between −180° and −90°, corresponding to capacitive and negative resistance characteristics. Notably, under both control strategies, adding delay compensation causes MMC to behave as a capacitance at frequencies around n/T_d. Under power control, the steady-state operating point of MMC has minimal impact on high-frequency impedance. However, under DC voltage control, the capacitive regions are slightly wider when MMC operates in inverter mode than in rectifier mode, and the regions expand with higher inverter output power. The results align with the previous theoretical analysis.

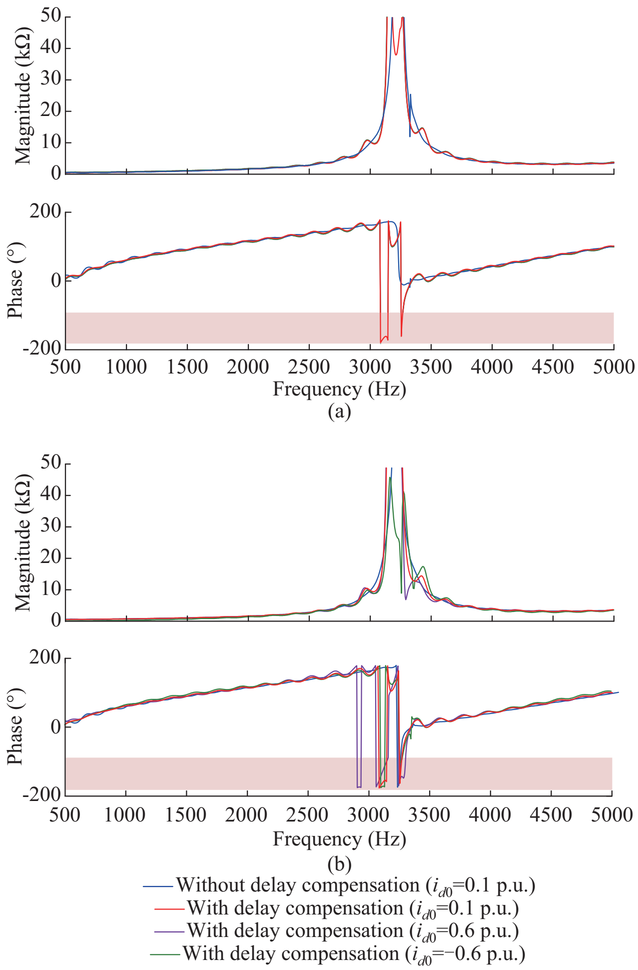

Fig. 9. MMC impedances with and without delay compensation for varying i_{d0} values under different control strategies. (a) Under power control. (b) Under DC voltage control.

The above analysis shows that delay compensation is a critical factor for MMC to exhibit capacitive characteristics in the frequency range of several kilohertz. The simulations of Scenario 2 presented in Section II-B also confirm this finding. Therefore, when adopting delay compensation in practical engineering applications, it is crucial to incorporate this factor into MMC impedance model for precise HFO analysis.

C. Effects of Frequency Dependence of AC Line Parameters

The AC network also plays a critical role in the occurrence of HFOs. The frequency dependence of AC line parameters can significantly influence HFO analysis results. An illustrative example is presented as follows. The line length is set to be 50 km, with other parameters the same as those in Table I.

Figure 10 compares the analytical impedances with and without considering the frequency dependence of AC line parameters. Note that when the frequency dependence of AC line parameters is considered, no magnitude intersection with a phase difference exceeding 180° occurs between MMC and AC network impedances, indicating system stability.

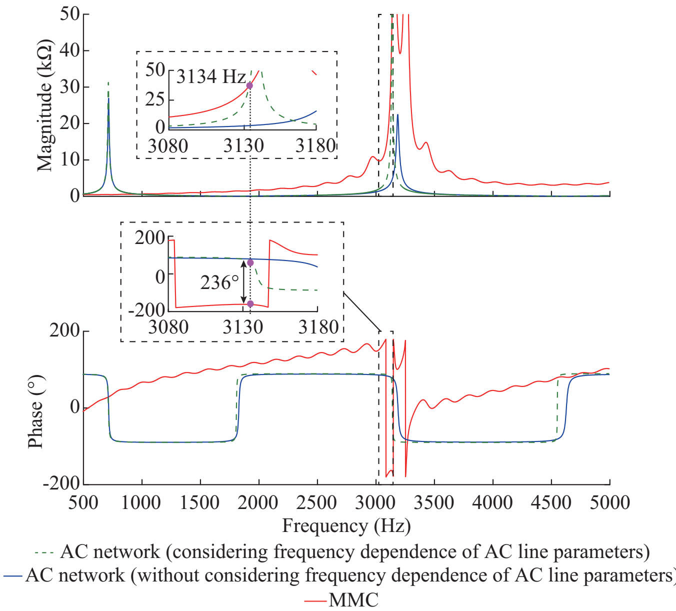

Fig. 10. Analytical impedances with and without considering frequency dependence of AC line parameters.

However, when the frequency dependence of AC line parameters is not considered, the second magnitude peak of AC network occurs at a lower frequency and reaches a much higher value. As a result, a magnitude intersection between MMC and AC network impedances occurs at 3134 Hz, and the phase difference is above 180°, indicating system instability. It is indicated that the frequency dependence of AC line parameters significantly affects impedance characteristics of AC network, and thus HFO analysis results.

V. Discussions

A. Potential Multiple HFOs

The new HFO phenomenon arises from the interaction between capacitive impedance of MMC and inductive impedance of AC network, which differs from the mechanism of conventional HFOs. Yet, it is noteworthy that multiple HFOs, including both the new and conventional HFOs, may occur simultaneously. The following example illustrates this co-occurrence.

Parameters in Table I are used again, yet with k_p set to be 2.8 and the length of AC overhead line set to be 2.5 km. Figure 11 shows the analytical impedances of MMC and AC network, revealing two unstable HFOs at 686 Hz and 4753 Hz. The occurrence mechanisms of these two HFOs are different. For the HFO at 686 Hz, MMC exhibits capacitive characteristics and AC network exhibits inductive characteristics. In contrast, for the HFO at 4753 Hz, MMC exhibits inductive characteristics and AC network exhibits capacitive characteristics, indicating it is a conventional HFO.

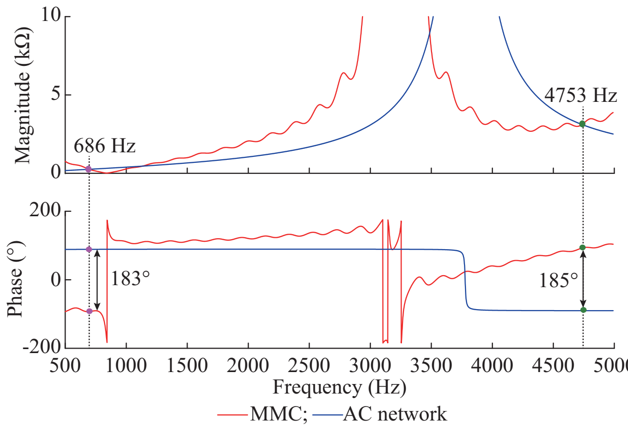

Fig. 11. Analytical impedances of MMC and AC network.

Figure 12 presents the simulation results of multiple HFOs. Initially, the time delay of MMC is set to be 10 μs; and at $t=1$ s, the time delay is switched to 300 μs, triggering unstable oscillations, as shown in Fig. 12(a). A three-dimensional plot of DFT analysis results is depicted in Fig. 12 (b). Obviously, there are two coexisting HFOs at 682 Hz and 4748 Hz, both of which are gradually diverging. The simulation results support the theoretical analysis.

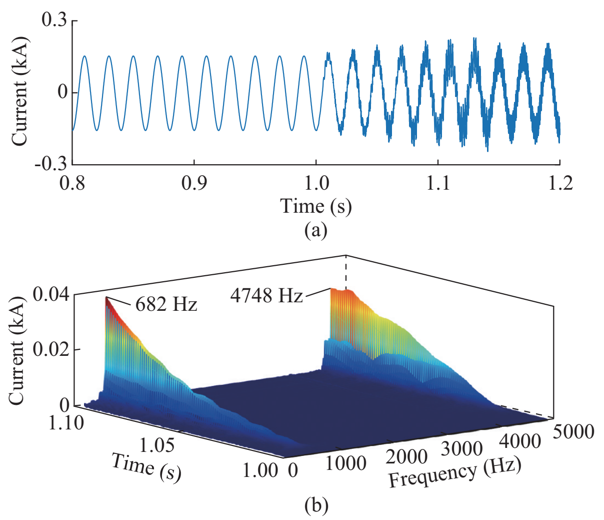

Fig. 12. Simulation results of multiple HFOs. (a) AC-side current of MMC-HVDC. (b) DFT analysis result.

Notably, both MMC and AC network can exhibit multiple capacitive and inductive regions in high-frequency range, resulting in complex interactions between them. These interactions may lead to co-occurrence of multiple HFOs with different occurrence mechanisms.

It is worth noting that, in addition to overhead lines, AC networks may also employ cables. Due to the significantly higher distributed capacitance of cables, the first resonance peak of a cable appears at a lower frequency than that of an overhead line with the same length [28]. Meanwhile, the higher distributed capacitance in cables leads to more frequent transitions between inductive and capacitive regions in high-frequency range. It may increase the risk of multiple HFOs occurring simultaneously.

B. Possible Mitigation Approaches

The complexity of HFO dynamics highlights the need for advanced mitigation approaches. Here are some discussions on possible countermeasures.

1) Optimizing control parameters of MMC: Section IV-B reveals that the proportional gains of current and power controls significantly influence MMC impedance characteristics. By appropriately reducing these parameters without affecting the normal control performance of MMC, the HFO risk in the frequency range of 500 Hz to 1000 Hz could be reduced. However, for HFOs in the higher frequency range of several kilohertz, optimizing control parameters alone is insufficient.

2) Improving control scheme of MMC: embedding a low-pass filter (LPF) into the voltage feedforward path of MMC is a conventional approach to mitigating HFOs. However, LPF fails to fully eliminate high-frequency negative damping and may introduce new risky regions [29], posing HFO risks during grid topology transitions or parameter variations.

Given the sensitivity of HFOs to operating conditions, effective mitigation of HFOs requires adaptive solutions. Recent studies propose adding adaptive narrowband damping loops [7], [30] or notch filters [29], [31] into existing MMC control scheme. These additions can modify MMC impedance at the detected HFO frequencies, thereby stabilizing single or multiple HFOs under variable operating conditions.

3) Using grid-side damping controllers*:* grid-side damping controllers can also be employed to mitigate HFOs. One such approach is connecting a shunt converter with adaptive damping loops, like the subsynchronous damper introduced in [32], [33]. By injecting currents at single or multiple HFO frequencies, the shunt converter can reshape the equivalent system impedance, thus stabilizing HFOs. This approach is also adaptable to variable operating conditions.

VI. Conclusion

This paper reveals a new HFO phenomenon in MMC-HVDC connected to AC networks, investigating its modeling and mechanism. The following conclusions are drawn.

1) In high-frequency range, MMC can exhibit capacitive characteristics with negative resistance, and its interaction with AC networks (behaving inductively) can potentially trigger a new HFO risk. This HFO risk exists irrespective of whether MMC-HVDC is connected to short or long AC lines.

2) MMC may exhibit two types of capacitive regions in high-frequency range, and the causes are theoretically ex-

plained. The first type is associated with the relatively high proportional gains of current and outer-loop controls, especially under power control. The second type is related to the addition of delay compensation and is also influenced by the active power output under DC voltage control.

3) A practical modeling method for AC lines is proposed, employing a numerical approximation technique to accurately capture the frequency dependence of AC line parameters. Case study shows that neglecting this frequency dependence in models would lead to wrong assessments of HFOs.

4) In some situations, MMC-HVDC connected to AC networks may encounter multiple coexisting HFOs with different occurrence mechanisms. Possible mitigation approaches for those HFOs are discussed for further investigation.

References

[1] F. Martinez-Rodrigo, D. Ramirez, A. Rey-Boue *et al*., "Modular multilevel converters: control and applications," *Energies*, vol. 10, no. 11, p. 1709, Nov. 2017.

[2] S. Debnath, J. Qin, B. Bahrani *et al*., "Operation, control, and applications of the modular multilevel converter: a review," *IEEE Transactions on Power Electronics*, vol. 30, no. 1, pp. 37-53, Jan. 2015.

[3] H. Saad, Y. Fillion, S. Deschanvres *et al*., "On resonances and harmonics in HVDC-MMC station connected to AC grid," *IEEE Transactions on Power Delivery*, vol. 32, no. 3, pp. 1565-1573, Jun. 2017.

[4] J. Man, X. Xie, S. Xu *et al*., "Frequency-coupling impedance model based analysis of a high-frequency resonance incident in an actual MMC-HVDC system," *IEEE Transactions on Power Delivery*, vol. 35, no. 6, pp. 2963-2971, Dec. 2020.

[5] C. Zou, H. Rao, S. Xu *et al*., "Analysis of resonance between a VSC-HVDC converter and the AC grid," *IEEE Transactions on Power Electronics*, vol. 33, no. 12, pp. 10157-10168, Dec. 2018.

[6] Y. Li, T. An, D. Zhang *et al*., "Analysis and suppression control of high frequency resonance for MMC-HVDC system," *IEEE Transactions on Power Delivery*, vol. 36, no. 6, pp. 3867-3881, Dec. 2021.

[7] J. Sun, I. Vieto, and C. Buchhagen, "High-frequency resonance in HVDC and wind systems: root causes and solutions," *IET Renewable Power Generation*, vol. 17, no. 14, pp. 3507-3522, Oct. 2023.

[8] T. Huang, F. Yang, D. Zhang *et al*., "High-frequency stability analysis and impedance optimization for an MMC-HVDC integrated system considering delay effects," *IEEE Journal on Emerging and Selected Topics in Circuits and Systems*, vol. 12, no. 1, pp. 59-72, Mar. 2022.

[9] Z. Xu, B. Li, X. Wang *et al*., "High-frequency resonance suppression based on unified MMC high-frequency impedance model," *IEEE Transactions on Power Electronics*, vol. 37, no. 12, pp. 14755-14769, Dec. 2022.

[10] J. Zhu, J. Hu, L. Lin *et al*., "High-frequency oscillation mechanism analysis and suppression method of VSC-HVDC," *IEEE Transactions on Power Electronics*, vol. 35, no. 9, pp. 8892-8896, Sept. 2020.

[11] S. Zhu, K. Liu, X. Liao *et al*., "*D-Q* frame impedance modeling of modular multilevel converter and its application in high-frequency resonance analysis," *IEEE Transactions on Power Delivery*, vol. 36, no. 3, pp. 1517-1530, Jun. 2021.

[12] Y. Li, T. Wen, Y. Cao *et al*., "High-frequency resonance coordinated suppression method of MMC-HVDC systems under frequency divided voltage feedforward control," *IEEE Transactions on Power Delivery*, vol. 40, no. 2, pp. 938-950, Apr. 2025.

[13] Y. Li, H. Pang, M. Kong *et al*., "Compensation control and parameters design for high frequency resonance suppression of MMC-HVDC system," *CSEE Journal of Power and Energy Systems*, vol. 7, no. 6, pp. 1161-1175, Nov. 2021.

[14] C. Zou, J. Chen, S. Xu *et al*., "Dynamic performance optimization of VSC-HVDC considering its long delay," *Power System Technology*, vol. 41, pp. 3216-3222, Oct. 2017.

[15] X. Zhao, H. Qin, J. Feng *et al*., "Improvement effect of delay compensation on high-frequency resonance characteristics of MMC-HVDC," in *Proceedings of 2024 9th Asia Conference on Power and Electrical Engineering*, Shanghai, China, Apr. 2024, pp. 256-262.

[16] G. Song, X. Chu, S. Gao *et al*., "Novel distance protection based on distributed parameter model for long-distance transmission lines," *IEEE Transactions on Power Delivery*, vol. 28, no. 4, pp. 2116-2123, Oct. 2013.

[17] Y. Song, E. Ebrahimzadeh, and F. Blaabjerg, "Analysis of high-frequency resonance in DFIG-based offshore wind farm via long transmission cable," *IEEE Transactions on Energy Conversion*, vol. 33, no. 3, pp. 1036-1046, Sept. 2018.

[18] P. Huang and L. Vanfretti, "Multi-tuned narrowband damping for suppressing MMC high-frequency oscillations," *IEEE Transactions on Power Delivery*, vol. 38, no. 6, pp. 3804-3819, Dec. 2023.

[19] M. Akke and T. Biro, "Measurements of the frequency-dependent impedance of a thin wire with ground return," *IEEE Transactions on Power Delivery*, vol. 20, no. 2, pp. 1748-1752, Apr. 2005.

[20] S. Kurokawa, J. Pissolato, M. C. Tavares *et al*., "A new procedure to derive transmission-line parameters: applications and restrictions," *IEEE Transactions on Power Delivery*, vol. 21, no. 1, pp. 492-498, Jan. 2006.

[21] I. Jurić -Grgić, A. Bernadić, and R. Lucić, "Time-domain finite element method analysis of frequency-dependent transmission lines," *IEEE Transactions on Electromagnetic Compatibility*, vol. 58, no. 1, pp. 287-293, Feb. 2016.

[22] J. Svensson, M. Bongiorno, and A. Sannino, "Practical implementation of delayed signal cancellation method for phase-sequence separation," *IEEE Transactions on Power Delivery*, vol. 22, no. 1, pp. 18-26, Jan. 2007.

[23] T. Yin, Y. Wang, J. Sun *et al*., "Impedance-based characterization of positive-negative sequence separation and its effects on MMC-HVDC stability," *IEEE Journal of Emerging and Selected Topics in Power Electronics*, vol. 10, no. 4, pp. 4395-4412, Aug. 2022.

[24] H. Li, J. Shair, J. Zhang *et al*., "Investigation of subsynchronous oscillation in a DFIG-based wind power plant connected to MTDC grid," *IEEE Transactions on Power Systems*, vol. 38, no. 4, pp. 3222-3231, Jul. 2023.

[25] B. Gao, Y. Wang, W. Xu *et al*., "Identifying and ranking sources of SSR based on the concept of subsynchronous power," *IEEE Transactions on Power Delivery*, vol. 35, no. 1, pp. 258-268, Feb. 2020.

[26] S. Vujević, D. Lovrić, and V. Boras, "High-accurate numerical computation of internal impedance of cylindrical conductors for complex arguments of arbitrary magnitude," *IEEE Transactions on Electromagnetic Compatibility*, vol. 56, no. 6, pp. 1431-1438, Dec. 2014.

[27] W. Mingli and F. Yu, "Numerical calculations of internal impedance of solid and tubular cylindrical conductors under large parameters," *IEE Proceedings: Generation*, *Transmission and Distribution*, vol. 151, no. 1, p. 67, Jan. 2004

[28] H. Khalilnezhad, M. Popov, L. van der Sluis *et al*., "Influence of long EHV AC underground cables on the resonance behavior of the Dutch transmission system," in *Proceedings of 2016 IEEE PES General Meeting*, Boston, USA, Jul. 2016, pp. 1-5.

[29] C. Guo, D. Du, H. Cheng *et al*., "A frequency estimation-based adaptive mitigation approach for high-frequency oscillation in MMC-HVDC system," *IEEE Transactions on Power Systems*, vol. 39, no. 4, pp. 5509-5521, Jul. 2024.

[30] P. Huang and L. Vanfretti, "Adaptive damping control of MMC to suppress high-frequency resonance," *IEEE Transactions on Industry Applications*, vol. 59, no. 6, pp. 7224-7237, Nov.-Dec. 2023.

[31] J. Man, L. Chen, V. Terzija *et al*., "Mitigating high-frequency resonance in MMC-HVDC systems using adaptive Notch filters," *IEEE Transactions on Power Systems*, vol. 37, no. 3, pp. 2086-2096, May 2022.

[32] J. Shair, X. Xie, H. Li *et al*., "A grid-side multi-modal adaptive damping control of super-/sub-synchronous oscillations in type-4 wind farms connected to weak AC grid," *Electric Power Systems Research*, vol. 215, p. 108963, Feb. 2023.

[33] X. Zhang, X. Xie, J. Shair *et al*., "A grid-side subsynchronous damping controller to mitigate unstable SSCI and its hardware-in-the-loop tests," *IEEE Transactions on Sustainable Energy*, vol. 11, no. 3, pp. 1548-1558, Jul. 2020.

Jieyi Xu received the B.S. degree in electrical engineering from Tsinghua University, Beijing, China, in 2022, where she is currently working toward the Ph.D. degree. Her research interests include dynamic stability and control of power systems with high penetration of renewable energy sources and power electronics.

Hui Qin received the M.S. degree from Wuhan University, Wuhan, China, in 2006. She is currently a Manager of Planning Center of Guangxi Power Grid Co., Ltd., Nanning, China. Her research interests include power grid

planning and stability analysis.

Wenkai Dong received the Ph. D. degree in electrical engineering from North China Electric Power University, Beijing, China, in 2021. He is currently an Assistant Researcher of the State Key Laboratory of Power System Operation and Control, Tsinghua University, Beijing, China. His research interests include power system dynamics and control.

Juan Chen received the B. S. degree from Guangxi University, Nanning, China, in 2014. She is currently a Supervisor of Qinzhou Power Supply Bureau, Guangxi Power Grid Co., Ltd., Nanning, China. Her research interests primarily focus on power grid planning.

Xiaorong Xie received the Ph.D. degree from Tsinghua University, Beijing, China, in 2001. He is currently a Professor of Department of Electrical Engineering, Tsinghua University. His research interests include dynamic analysis and control of power systems, especially those with high penetration of renewable energy sources and power electronics.